detected by observing backscattered light, although the reflection is not always large.

Fractured sections of the fibres were observed by scanning electromicroscope. Typical micrographs are shown in Fig. 4.

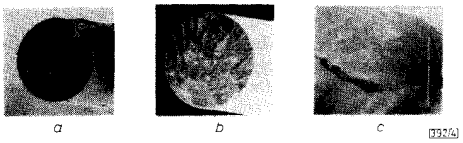

Fig. 4 *Micrographs of fractured sections of fibres*
a Example of small loss increase sample (loss increase 0·01 dB)
b Example of high loss increase sample (loss increase 8·1 dB)
c Example of fracture caused by twisting stress (loss increase more than 40 dB)

The results are as follows.

(1) The fractured section of the sample, in which the loss increase caused by tensile stress and bending stress is small, has a mirror zone only. The fractured section is almost perpendicular to the fibre axis.

(2) The fractured section of the sample in which the loss increase caused by bending stress is large has a small mirror zone and a big hackle zone. The core part of the fibre is in the hackle zone. The hackle zone is slightly oblique to the fibre axis.

(3) The fractured section of the sample in which the loss increase caused by twisting stress is very large has swirled hackles. The fractured section is oblique to the fibre axis.

Axis misalignment of the fractured sections is observed in an X-ray photograph of the fibre. Large axis misalignment is observed in the parts fractured by twisting stress, as shown in Fig. 5. On the other hand, no axis misalignment is observed in the parts fractured by tensile stress and bending stress.

Fig. 5 *X-ray photograph of axis misalignment of fibre fractured by twisting stress*

These results show that the wide mirror zone, which contains the core part, is necessary for small loss increase. The mirror zone size is given by eqn. 1.[3]

$$Z \cdot R^{1/2} = K \quad (1)$$

where Z is the fracture stress, R is the distance from the original point to the mirror zone boundary, and K is a constant for a given material (7·5 kg/mm^2 for fused silica). Because the fibre diameter and the core diameter of the test fibre are approximately 0·125 mm and 0·01 mm, respectively, R should be greater than 0·0675 mm to cover the core part with the mirror zone. The Z which gives this value is 29 kg/mm^2, calculated by eqn. 1. The percentage of the splicing sections in which fracture stress is under this value is assumed to be approximately 10%.[4] This calculated result does not correspond to the experimental results shown in Table 1, because all samples fractured by tensile stress and 70% of the samples fractured by bending stress show a small loss increase.

This point is worth investigating in detail in the future.

Conclusion: It is discovered experimentally that the optical loss increase of the fractured splice of the optical fibres caused by tensile stress and bending stress is small, whereas that caused by twisting stress is large. For a small loss increase, an optical transmission circuit can be maintained without breakdown by detecting and repairing the fractured section after the fracturing. The fractured section can be detected by measuring the backscattered light of the fibre.

The existence of the fractured splicing section in which loss increase is small is also a warning that the fracturing could occur and be overlooked.

Acknowledgment: The authors would like to thank K. Ishihara for his encouragement and K. Arakawa for his useful discussion.

T. KUWABARA
H. KOGA
Y. MISTUNAGA
S. ISOBE

NTT Telecommunication Field Systems R&D Center
Nippon Telegraph and Telephone Corporation
Tokai-mura, Ibaraki, 319-11, Japan

23rd July 1991

References

1 TOMITA, S., and SUTOU, K.: 'Optical loss variation due to fiber handling at the joining point on the subscriber loop', *Trans. IEICE of Japan*, 1991, **J74-B-I**, (2), pp. 144–150
2 SUTO, K., BANDA, Y., TOMITA, S., and TSUCHIYA, T.: 'Optical receiver design considering fiber loss fluctuation for subscriber loops', *Trans. IEICE of Japan*, 1991, **E-74**, (3), pp. 547–554
3 GLOGE, D., SMITH, P. W., BISBEE, D. L., and CHINNOCK, E. L.: 'Optical fiber end preparation for low-loss splices', *Bell Syst. Tech. J.*, 1973, **52**, (9), pp. 1579–1588
4 MATSUMOTO, M., HAIBARA, H., KATSUYAMA, Y., MIYAUCHI, M., TOKUDA, M., and TANIFUJI, T.: 'Long-term reliability assurance for arc-fusion spliced fiber', *Trans. IECE of Japan*, 1984, **J67-B**, (5), pp. 521–528

GENERAL NEURAL UNIT: RETRIEVAL PERFORMANCE

Indexing term: Neural networks

A general neural unit is described which is capable of retrieving learned prototype images at internal connections when stimulated by distorted versions of the prototypes at the external terminals. Theoretical predictions of optimal feedback for best retrieval performance are given with experimental confirmation.

Introduction: The general neural unit (GNU) as shown in Fig. 1 has been introduced as a building brick for neural systems.[1] This consists of K neural nodes of the weightless G-RAM variety (labelled G in Fig. 1). Lucy[2] has shown that effective storage and retrieval may be obtained in systems that are fully interconnected and have no external inputs (i.e. in terms of Fig. 1, $a = n = K$ and $i = 0$). However, such systems may have

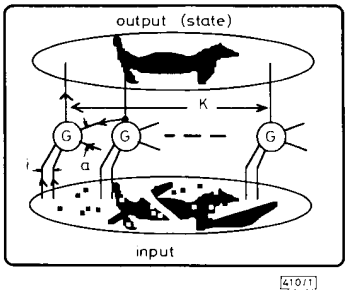

Fig. 1 *General neural unit*

to be deployed in pattern association tasks where a large number of nodes are required and maintaining $n = K$ would imply too high a node cost. Also, it is appropriate to account for external inputs to the system (nonzero i). Thus, in this Letter, a cost limitation is introduced in the sense that the number of inputs n for each node is constant, whereas the degree of feedback a, traded off against inputs i, is a variable ($n = i + a$). The question considered in this Letter is the way in which retrieval performance is affected by this tradeoff. All connections are assumed to be fixed, but randomly chosen.

Theory and framework: For clarity, it is first assumed that only two binary prototype patterns are involved: the all-white (all-0) pattern W and the all-black (all-1) pattern B. The system is trained first with W on both the input and internal terminals and this is repeated for B. An ideal associator is expected to retrieve W or B at the internal terminals depending on whether the input pattern is predominantly W or B, respectively. It is assumed that during any test, the proportion of 1s in the input image is b and the proportion of 1s generated at the internal terminals is p. At the beginning of a test p is assumed to have a value of 0·5.

G-RAMs are flexible neural devices for which a generalisation algorithm and an output resolution must be stated. Here it is assumed that the output resolution is three: 0, 1 and equal probability of generating a 0 or a 1. This third state is usually[2] given the label u. The G-RAM starts with all its locations in the u state. Training causes some locations (as addressed by the training patterns) to store and subsequently output a 1, others doing the same with a 0. The generalisation here is such that any location remaining in the u state after training is set to the value of the location with the most similar address and non-u location. Locations with nearest addresses that store conflicting training data are left in the u state. For the B and W training patterns in the current example the all-0 addresses store a 0 and the all-1 addresses are set to 1; then, after generalisation takes place, all addresses with a majority of 1s will be set to 1, all addresses with a majority of 0s to 0 and, for n even, addresses with equal numbers of 0s and 1s remain at u.

In contrast with the Lucy system,[2] the GNU in this case is synchronous, all nodes being capable of changing output at the arrival of a clock pulse. The notation is adopted where p is used at time t and p' for the next value at $t + 1$. The dynamics of the GNU are revealed by calculating p' as a function of p with b, i and a as the parameter of the system.

The probability of obtaining y 1s at i terminals is

$$P(y, i, b) = \binom{i}{y} b^y (1 - b)^{i-y} \tag{1}$$

Using a similar notation we have $P(z, a, p)$ as the probability of obtaining z 1s at the a terminals. Now, for n an odd integer, p' is given by

$$p'(odd) = \sum_{y=0}^{i} \sum_{z=0\cdot5(n+1)-y}^{a} P(y, i, b) \,.\, P(z, a, p) \tag{2}$$

If n is even there is an additional group of nodes $P(h, a, p)$ (where h is $0{\cdot}5a - y$) whose u contents are addressed. Half of these are likely to output a 1, hence p' for this case is

$$p'(even) = \sum_{y=0}^{i} \sum_{z=0\cdot5n-y+1}^{a} P(y, i, b) \times [P(z, a, p) + 0{\cdot}5P(h, a, p)] \tag{3}$$

Predictions: Eqns. 2 and 3 are often[3] called retrieval equations. To illustrate the properties of such equations (and hence predict the performance of the GNU), a specific case is considered for $K = 64$ and $n = 8$. The input pattern is randomly chosen to be 9/16 black (i.e. 1/16 above half 1s). In Fig. 2, p' against p is shown for different values of i as calculated from eqn. 3. The salient features of these curves are the intersections with the $p' = p$, 45° diagonal (e.g. X and Y in Fig. 2). The upper crossing point is a stable attractor of neighbouring values of p. Curves with a crossing point such as X would predict a settling at X rather than the all-1 state. Although this represents retrieval of the correct pattern it also shows a small error (noise) in the retrieved pattern. On the other hand, points such as Y are metastable repellers, so that if p is below Y, the system is predicted to settle in the all-0 state (which is an error of retrieval).

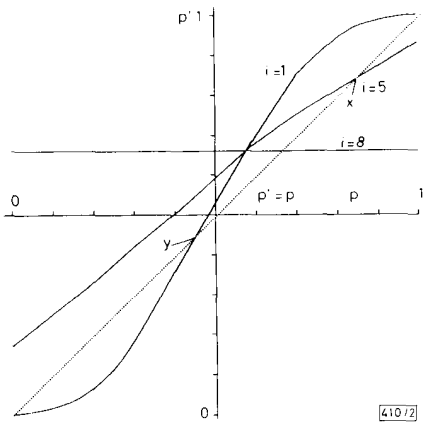

Fig. 2 *Examples of retrieval equation*

It may be shown that crossing point Y disappears when p' in eqn. 3 is nonzero for $p = 0$. This can only happen when z is zero or h is zero. The latter is more stringent and occurs only if $i \geq n/2$, i.e. $i \geq 4$, in the example above. In contrast, crossing point X appears when p' in eqn. 3 is less than 1 for $p = 1$. This also happens for $i \geq n/2$. It is also evident that X is at its highest value for $i = n/2$. This therefore is an optimum value for i.

A further prediction that can be made from eqn. 3 (this was done numerically in this case) is the actual value of p' at X.

Table 1 PERFORMANCE

i	1	2	3	4	5	6	7	8
$m(Y)$%	15	12	10	4	2	0	0	0
$m(X)$%	100	100	100	95	81	72	67	63
$p(X)$%	100	100	100	96	82	70	65	63
Perf	85	88	90	91	79	72	67	63

Practical results: These are shown in Table 1 in which the measured probability of ending in the wrong state due to the presence of Y is $m(Y)$, the measured final accuracy due to X is $m(X)$ and the predicted value of p at X is $p(X)$. An overall performance figure $Perf = m(X) - m(Y)$ shows the predicted performance peak for $i = 4$. The correspondence between measured and predicted retrieval accuracies at Y also indicates that the model of eqn. 3 has captured the mechanisms that are at work.

Finally, some results are presented for the nonorthogonal patters shown in Fig. 3. Here three patterns have been used

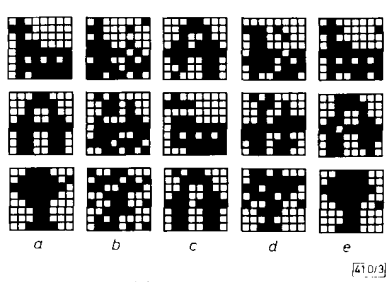

Fig. 3 *Retrieval of three patterns*

a Training
b Noise-distorted input
c Typical retrieval error with $i = 1$
d Noisy retrieval with $i = 8$
e Optimal retrieval with $i = 4$

for training. This is well below the limit for which interference would be expected in training from patterns that provide the same input for some G-RAM but demand different outputs.[4] It is seen again that $i = 4$ provides optimal retrieval.

Conclusion: It has been shown both theoretically and confirmed practically that the general neural unit has an optimal retrieval performance when each node receives as many inputs from the input field as from the feedback field.

I. ALEKSANDER *25th July 1991*

Department of Electrical and Electronic Engineering
Imperial College of Science Technology and Medicine
London SW7 2BT, United Kingdom

H. B. MORTON

Department of Human Sciences
Brunel University
Uxbridge, Middlesex, UB8 3PH, United Kingdom

References

1 ALEKSANDER, I.: 'Neural systems engineering: towards a unified design discipline?', *IEE Compl & Cont. J.*, 1990, **1**, pp. 259–265
2 LUCY, J.: 'Perfect autoassociators using RAM-type nodes', *Electron. Lett.*, 1991, **27**, pp. 799–800
3 WONG, K. Y. M., and SHERRINGTON, D.: 'Storage properties of Boolean neural networks'. Proc. nEuro 88, Paris, 1988, pp. 424–433
4 NTOURNTOUFIS, P.: 'Storage capacity and retrieval properties of an auto-associative general neural unit'. Proc. IJCNN, Seattle, 1991, p. 959

GAIN-SWITCHED LASER-AMPLIFIER PHOTONIC INTEGRATED CIRCUIT GENERATING 590 mW PEAK POWER OPTICAL PULSES

Indexing terms: Amplifiers, Integrated optics, Pulse generation, Semiconductor lasers, Optics

Gain-switching a strained-layer multiple quantum well laser-amplifier photonic integrated circuit has produced optical pulses with durations of 28 ps and peak powers of 590 mW (i.e. pulse energies of 21 pJ). The device was gain-switched at frequencies from 2 to 8 GHz. Such monolithic high-power pulse sources are of great importance for nonlinear fibre device applications.

High-power pulse sources are needed for such applications as switching and demultiplexing employing fibre nonlinearities.[1,2] Previously, high-power pulse trains have been obtained by external amplification, often using Er^{3+}-doped fibre amplifiers. However, monolithic integrated multiple quantum well (MQW) amplifiers can advantageously be employed as booster amplifiers. MQW amplifiers offer high saturation powers.[3] Furthermore, by integrating the amplifier with the source, the issue of polarisation sensitivity is eliminated. Photonic integrated circuits (PICs) combining lasers and booster amplifiers have been demonstrated for increasing the power from photonic integrated transmitters[4–6] and as pump sources for Er^{3+}-doped fibre amplifiers.[7] We present results on obtaining high-power picosecond pulses from a PIC by gain-switching the laser section and boosting the pulse amplitude by means of the integrated amplifier. Pulses with peak powers of up to 590 mW into air, 260 mW coupled into a fibre, and durations of 28 ps have been obtained at a repetition rate of 3·0 GHz. The PIC was successfully gain-switched in the frequency range from 2 to 8 GHz.

A schematic diagram of the PIC, which includes a distributed Bragg reflector (DBR) laser and a high-saturation-power amplifier, is shown in Fig. 1. The laser cavity is formed between a cleaved facet, onto which a highly-reflective (HR) coating has been applied, and a partially reflecting Bragg mirror. The lengths of the active laser section and the grating are 275 μm and 120 μm, respectively. The width of the laser waveguide is 2·5 μm. The DBR laser exhibits a threshold current of 14·5 mA. A lateral tapered waveguide section then adiabatically expands the mode into a 5 μm wide and 675 μm long amplifier section. The active sections of both the laser and the amplifier consist of four strained-layer multiquantum wells with a thickness of ~30 Å separated by 80 Å thick barriers. The MQW amplifier provides a high gain level and saturation output power because of the large transverse dimension in the junction plane.[3] To increase the gain efficiency further, the laser has been designed to oscillate on the short-wavelength side of the gain peak.[3] Measurements on a similar device showed a small-signal gain of 18·5 dB and a saturation output power for the amplifier of 95 mW.[7] Finally, the mode is also expanded vertically to improve the coupling efficiency. Far-field FWHM angles of 18 and 24° in the lateral and vertical directions, respectively, have been reported for a similar device.[7] An antireflection (AR) coating has been applied to the front facet to minimise reflections.

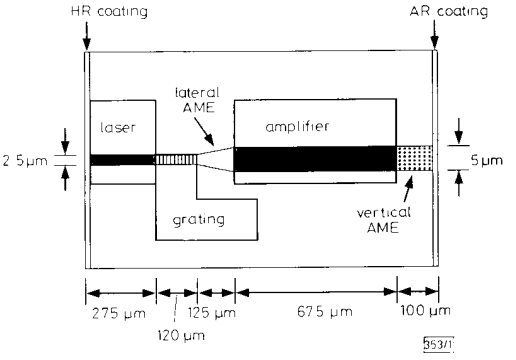

Fig. 1 *Schematic top view of laser-amplifier PIC*
AME: adiabatic mode expansion

In this experiment, we gain-switch the DBR laser by applying a sinusoidal drive superimposed on a DC current to the laser section. The amplifier is driven with a DC current. During measurements the PIC is kept at a constant temperature of 13°C. Peak powers and pulse energies are measured both at the facet and coupled into fibre. The device is sensitive to reflections because any backward-travelling light is amplified before being injected into the laser section. Therefore, great care must be taken to avoid reflections. When measuring the power at the facet, an AR coated spherical lens with a diameter of 2 mm is used for aiming the beam at a large-area detector. The spherical lens contributes very little loss and allows for neutral density filters to be inserted before the large-area detector. When coupling the beam onto fibre, an AR coated planoconvex GRIN-ROD lens is used for focusing the beam onto the bevelled end of a rotary connector. From these measurements we estimate an average coupling efficiency to fibre of $-3{\cdot}6 \pm 0{\cdot}5$ dB.

Fig. 2 shows the small-signal response at a laser current of 90 mA and an amplifier current of 250 mA, indicating a bandwidth of 7 GHz. The device has been gain-switched successfully at frequencies from 2 to 8 GHz. A streak camera recording of the pulse train, obtained at a repetition rate f_{rep} of 3·0 GHz, is shown in Fig. 3*a* with power into fibre as the vertical axis. The RF power P_{RF} and the DC current I_{laser} applied to the laser are +32·0 dBm (measured into 50 Ω) and 81 mA, respectively. A DC current I_{amp} of 280 mA is applied to the amplifier. The pulse width and the peak power at the facet are 28 ps and 590 mW, respectively. In the fibre, we measure a peak power of 260 mW. The pulse energies are 21 pJ at the facet and 9·0 pJ in the fibre. In Fig. 3*b* the corresponding time-averaged optical spectrum is shown. The laser section oscillates in multiple modes and exhibits chirp, as is typical for gain-switched Fabry–Perot and DBR lasers. As can be seen in Fig. 3*a*, the pulses exhibit minor tails. However, the tails